Article

On-Surface Annulation Reaction Cascade for the Selective Synthesis of Diindenopyrene

Frank Eisenhut, Thomas Lehmann, Andreas Viertel, Dmitry Skidin, Justus Krüger, Seddigheh Nikipar, Dmitry A Ryndyk, Christian Joachim, Stefan Hecht, Francesca Moresco, and Gianaurelio Cuniberti

ACS Nano, **Just Accepted Manuscript** • DOI: 10.1021/acsnano.7b06459 • Publication Date (Web): 14 Nov 2017

On-Surface Annulation Reaction Cascade for the Selective Synthesis of Diindenopyrene

Frank Eisenhut,[1] Thomas Lehmann,[1] Andreas Viertel,[2] Dmitry Skidin,[1] Justus Krüger,[1] Seddigheh Nikipar,[1] Dmitry A. Ryndyk,[1,3] Christian Joachim,[4] Stefan Hecht,[2] Francesca Moresco,[1] and Gianaurelio Cuniberti[1,5]*

[1]Institute for Materials Science, Max Bergmann Center of Biomaterials, and Center for Advancing Electronics Dresden, TU Dresden, 01069 Dresden, Germany

[2]Department of Chemistry & IRIS Adlershof, Humboldt-Universität zu Berlin, Brook-Taylor-Str. 2, 12489 Berlin, Germany

[3]Bremen Center for Computational Materials Science, Universität Bremen, Germany

[4]GNS & MANA Satellite, CEMES, CNRS, 29 rue J. Marvig, 31055 Toulouse Cedex, France

[5]Dresden Center for Computational Materials Science (DCMS), TU Dresden, 01069 Dresden, Germany

*Corresponding author: francesca.moresco@tu-dresden.de

ABSTRACT

We investigated the thermally induced on-surface cyclization of 4,10-bis(2'-bromo-4'-methylphenyl)-1,3-dimethylpyrene to form the previously unknown, non-alternant polyaromatic hydrocarbon diindeno[1,2,3-cd:1′,2′,3′-mn]pyrene on Au(111) using scanning tunneling microscopy and spectroscopy. The observed unimolecular reaction involves thermally induced debromination followed by selective ring-closure to fuse the neighboring benzene moieties *via* a five-membered ring. The structure of the product has been verified experimentally as well as theoretically. Our results demonstrate that on-surface reactions give rise to unusual chemical reactivities and selectivities and provide access to non-alternant polyaromatic molecules.

Keywords: on-surface reaction, single-molecule chemistry, scanning tunneling microscopy (STM), non-alternant polyaromatic hydrocarbon, density functional theory, reaction mechanism

On-surface synthesis represents one possible strategy to tailor-make and precisely construct nanostructures in which molecules form large covalent networks with atomic precision or to synthesize molecules that are not achievable in solution.[1-4] The most investigated reaction in this field is the Ullmann-coupling.[5-7] In the course of this reaction, one or several halogen atoms are cleaved from the molecule thereby creating on-surface radicals which can form covalent bonds either intramolecularly or intermolecularly leading to cyclization or polymerization. Exploiting the latter pathway, molecular wires,[8-9] 2D networks,[6] as well as graphene nanoribbons have been obtained.[10-11] Despite the continuous drive to prepare large covalent structures from small molecular precursors on metal surfaces, the selective formation of specific non-polymeric, *i.e.* discrete, molecules *via* surface-induced intramolecular reactions is of interest. Recent examples include the reversible Bergmann cyclization, the generation of arynes, or the generation of anti-aromatic molecules.[12-15]

Furthermore, suitable molecular precursors are used to generate polyaromatic hydrocarbons (PAHs) on surfaces, allowing for their convenient characterization by scanning probe microscopy.[16-20] Of particular interest are non-alternant PAHs since the presence of odd-numbered, such as five-membered, rings can be seen as a topological defect and have been shown to reduce the overall aromaticity.[21] Recently, five-membered rings have been achieved by surface-assisted cyclodehydrogenation or elimination of hydrofluoric acid.[11, 22-23] In addition, other ways to synthesize non-alternant PAHs on surfaces have been presented.[24-26]

Here, we report the on-surface synthesis of diindenopyrene on Au(111) starting from 4,10-bis(2'-bromo-4'-methylphenyl)-1,3-dimethylpyrene ($Br_2Me_4Ph_2Py$). After thermally induced debromination, regioselective cyclization to yield two five-membered rings occurs predominantly. Although, oligoindenopyrenes have been synthesized in solution,[27]

diindenopyrene derivatives presented in this article have not been reported so far to our knowledge. In this work, we use scanning tunneling microscopy (STM) and spectroscopy (STS) to resolve the molecular structure and electronic resonances in detail. More insight into the on-surface reaction mechanism is obtained by density functional theory (DFT) and electron scattering quantum chemistry (ESQC) calculations.

RESULTS AND DISCUSSION

On-surface synthesis

On-surface experiments were performed starting by the deposition of a sub-monolayer of the $Br_2Me_4Ph_2Py$ precursor molecules (Figure 1(a)) on a clean Au(111) surface kept at room temperature. STM images were recorded at low temperature (T = 5 K) and under ultra-high vacuum (UHV) conditions. Figure 1(b) presents a constant-current STM image of a single precursor molecule.

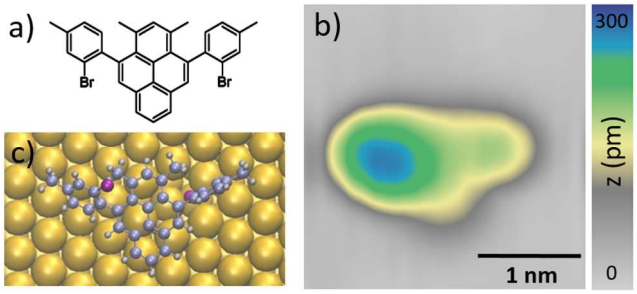

Figure 1. Precursor molecule adsorbed on Au(111). (a) Molecular structure of the precursor molecule 4,10-bis(2'-bromo-4'-methylphenyl)-1,3-dimethylpyrene ($Br_2Me_4Ph_2Py$). (b) STM image of a single isolated precursor molecule. The STM scan (V = + 1.0 V; I = 100 pA) shows that $Br_2Me_4Ph_2Py$ molecules appear asymmetric after adsorption on Au(111). (c) Ball-and-stick model of the fully relaxed $Br_2Me_4Ph_2Py$ molecule obtained by density functional theory (DFT) (colors: C-atoms: blue; Br-atoms: purple; H-atoms: grey).

As one can see in the STM image of Figure 1(b), one side of the molecule shows a larger conductance, *i.e.* appears higher than the other one, despite the symmetry of the molecular structure. To understand the adsorption conformation of the molecule, we performed density functional theory (DFT) calculations. These calculations show that the carbon-carbon bond between the pyrene core and the lateral phenyl rings is rather flexible. The $Br_2Me_4Ph_2Py$ precursor is mainly adsorbed in a non-planar conformation on the Au(111) surface with one of the bromine atoms pointing towards and the other bromine atom pointing away from the surface. This adsorption geometry explains the missing mirror symmetry and the significant apparent height difference within the molecule observed in the STM image.

At higher coverages, the $Br_2Me_4Ph_2Py$ molecules form one-dimensional chains along the fcc domain and row-like ordered monolayers (see Figure S1 in the Supporting Information).

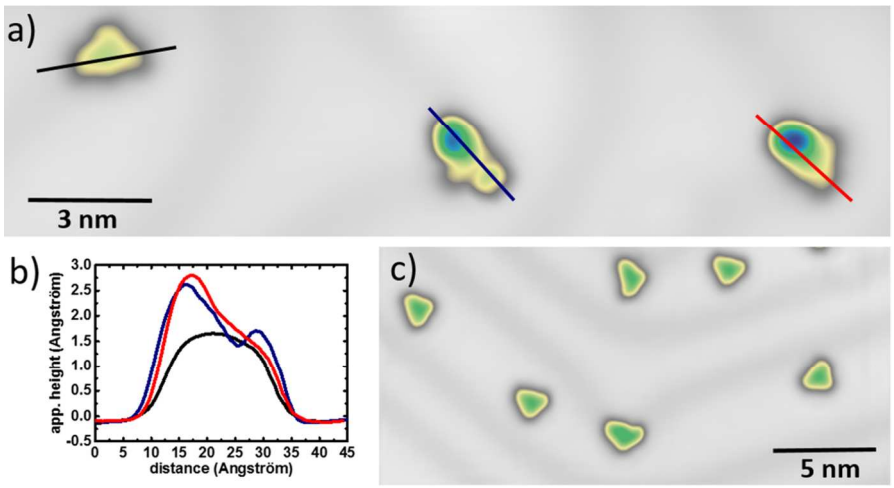

Figure 2. Debromination and planarization of $Br_2Me_4Ph_2Py$ molecules on Au(111). (a) STM image of three single isolated molecules after annealing to 160 °C for 5 min. The STM image (V = + 0.5 V; I = 100 pA) shows that isolated molecules with different shapes adsorb at the kink sites of the surface reconstruction. In the linescans in (b), taken along the molecules (marked in (a) with the same color), one can directly observe that precursor molecules, partially planar and completely planar molecules are on the surface after annealing. (c) STM image of several molecules after annealing to 200 °C. The STM image (V = + 0.5 V; I = 100 pA) shows that all

molecules have been planarized after the complete debromination of the molecules and no Ullmann-coupled structures have been observed.

To explore intramolecular on-surface chemical reactions using the $Br_2Me_4Ph_2Py$ precursor, the sample was annealed to 160 °C for 5 minutes. At this temperature, and as known from the literature,[28-32] a partial debromination is induced on Au(111). Figure 2(a) shows a STM image after this annealing. Three main molecular species are visible at the kink sites of the Au(111) herringbone reconstruction. At these defect points, the molecules are isolated on the surface. These three, approximately triangular, molecular species show large differences in their relative apparent height in the STM images. They have either two maxima, one maximum, or are completely planar, as shown by the line scan in Figure 2(b). We attribute the molecule with two maxima to the unreacted precursor $Br_2Me_4Ph_2Py$. Molecules having one maximum are partially planarized and are thus assigned to a reaction intermediate, while the fully planar molecule appears to correspond to a complete debrominated molecule. Beside the molecules at the kink sites, we also found larger structures on the surface. By STM lateral manipulation, we prove that these molecular structures are not covalently connected (see Figure S2 in the Supporting Information) and correspond to weakly bound supramolecular assemblies, similar to the ones observed after the precursor deposition but before heating. In addition and after annealing, we propose that these non-covalently bound dimer and tetramer molecular structures are formed from the partially planar intermediates by a halogen bond (see Figure S3 in the Supporting Information). Further byproducts were never observed on the surface.

After a further annealing step to 200 °C, all molecules appear planar on the surface (Figure 2(c)). At this temperature, the debromination is normally completed on Au(111).[28-32]

From our observations, we can conclude that debromination causes the planarization of the molecules induced by an efficient unimolecular reaction (Figure 3).

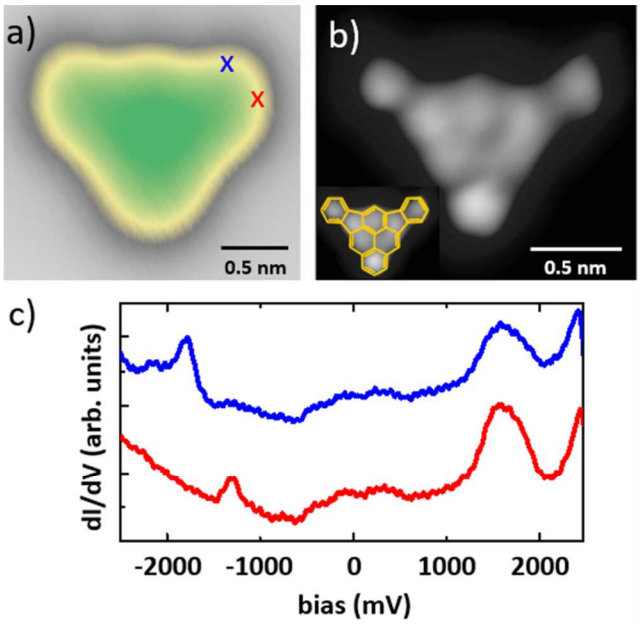

Figure 3. Imaging and spectroscopic measurement of single diindeno[1,2,3-cd:1′,2′,3′-mn]pyrene (DIP) molecules adsorbed on Au(111). (a) Close-up STM image (V = + 0.1 V; I = 100 pA) of DIP measured with a metallic tip. (b) DIP imaged with a CO-tip at constant height and V = + 10 mV. The inset shows the same molecule superimposed with the relaxed molecular structure of DIP. (c) Red and blue marks the position of point spectroscopy in (a) and the dI/dV spectra have been taken at constant height; the color of the curves matches with the color with the indicated tip position in (a). We observed resonances at -1.8 V, -1.3 V, +1.5 V and +2.45 V. The surface state of Au(111) is observed at -0.5 V. Tip heights were stabilized at V = + 0.5 V and I = 100 pA and the spectra range is from - 2.5 V to + 2.5 V.

To assign the molecular structure of the final product of the described on-surface reaction, we performed high-resolution STM imaging. Figure 3(a) presents a molecule measured with a metallic tip in constant current mode. By scanning this molecule with a CO-functionalized STM-tip in constant height mode,[33] we obtained the highly resolved image presented in Figure 3(b). We observe that two five-membered rings have been formed at the upper two bay regions of the pyrene core, giving rise to an indene formation. Since the planarity of the structure is

maintained, the formed pentagons lead to a bending between the two upper arms of the molecule. Note that the methyl groups, initially present in the $Br_2Me_4Ph_2Py$ precursor, disappeared in the final reaction product. We assign this on-surface synthesized, completely planar product molecule to a diindeno[1,2,3-cd:1′,2′,3′-mn]pyrene (DIP) molecule, which to the best of our knowledge has not been reported so far.

To investigate the electronic structure of the obtained DIP molecule, we have performed scanning tunneling spectroscopy (STS) with a metallic tip. Figure 3(c) shows the differential conductance spectra on single DIP molecules at the position marked by a red and a blue cross in Figure 3(a). We associate the conductance peaks at +1.5 V and -1.3 V to two tunneling electronic resonances that for simplicity we refer to as the lowest unoccupied molecular orbital (LUMO) and the highest occupied molecular orbital (HOMO), respectively (see discussion below). Within the bias voltage measurement range allowed by STM, we furthermore have access to two further well-defined electronic resonances at -1.8 V and +2.45 V that for simplicity again we refer to as HOMO-1 and LUMO+1, respectively. On other positions of the DIP molecule, no strong conductance peaks are observed.

Reaction mechanism

The proposed reaction path starting from the $Br_2Me_4Ph_2Py$ precursor and ending in DIP on Au(111) is summarized in Figure 4(a). The calculations show that after debromination, which is favored on the Au(111) surface in comparison to this reaction in gas phase,[34] the molecule cyclizes to form a five-membered instead of a six-membered ring (step 1). Comparing both processes, we see that although the reaction intermediate with only hexagonal rings in step 2 is about 0.3 eV lower in total energy, its formation energy barrier is 2.9 eV, *i.e.*, more than 1 eV

higher than for the five-membered ring. The key for this selectivity is the preferred reactivity of the debrominated radical species towards attack at the substituted phenyl position rather than the benzylic site of the nearby internal methyl group.[35] From the formed internal pentadienyl radical 2, the methyl group at the sp^3-carbon can migrate to the other, external methyl group, yielding the sterically less congested pentadienyl radical 3 (step 2). Subsequently, both methyl groups are combined and cleaved from the molecule, leaving one hydrogen atom at the initial site of the external methyl substitution (step 3). Since the observed, final product is symmetrical, this reaction sequence of cyclization, methyl migration and cleavage occurs subsequently within the other half of the molecule (steps 4-6), resulting in the final planar structure. The overall reaction appears to be driven by intramolecular strain release and an increase of the planarity of the π-system and hence stabilizing hybridization on the Au(111) surface.

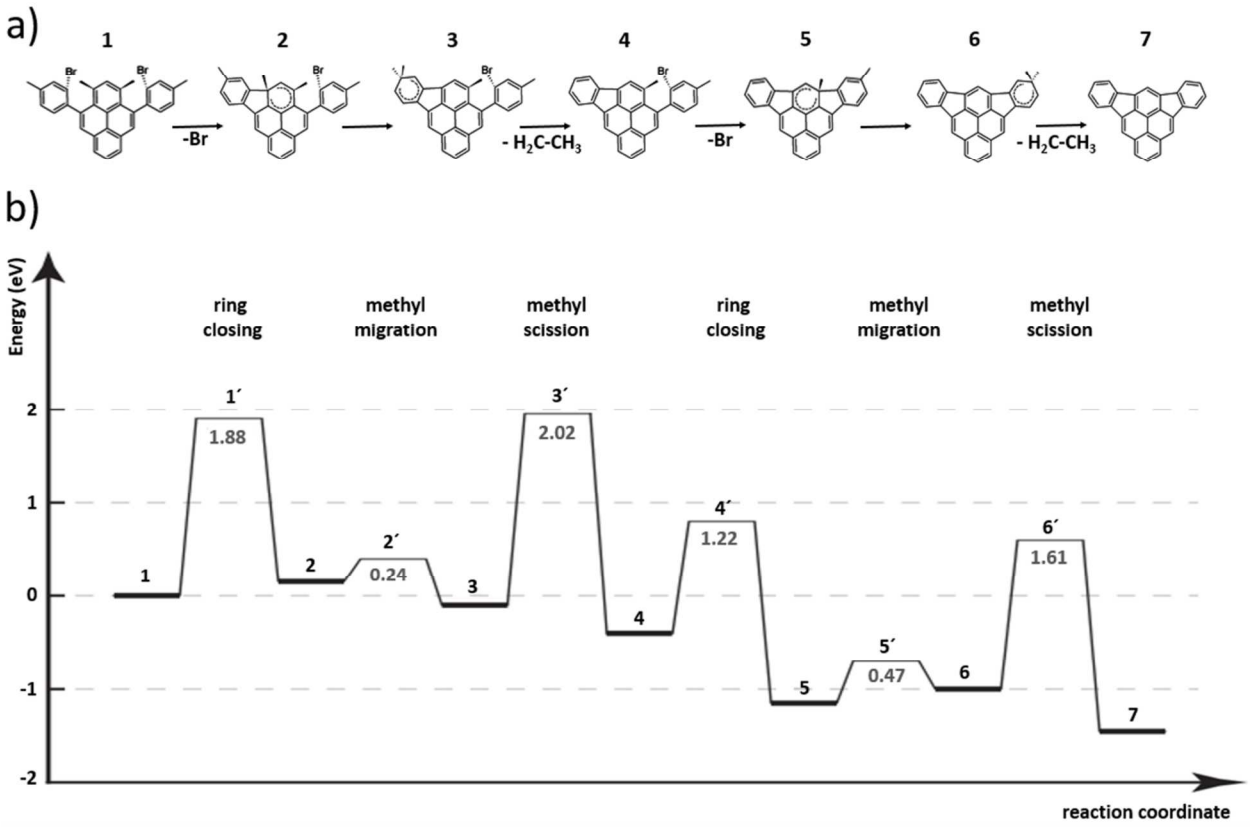

Figure 4. Reaction mechanism for the on-surface planarization of $Br_2Me_4Ph_2Py$ to form the planar DIP on Au(111). (a) Proposed reaction scheme and (b) Computed reaction energy diagram for all relevant species and transitions, based on *ab initio* climbing image-nudged elastic band (CI-NEB) calculations. The calculated effective barrier height is given in grey for each individual barrier in units of eV.

As indicated by the rather small chemical reaction barriers, the intermediates **2** and **5** have short lifetimes and consequently have not been observed in our experiments. In contrast and according to the relatively high barriers for the geminal-dimethyl cleavage, we suppose that some of the nonsymmetrical molecules imaged by STM (as for example in Figure 2(c)) are in fact intermediates **3** and **6**. Solely from the images a decisive differentiation is not possible. However, all calculated reaction barriers show values lower than 2 eV, *i.e.*, all steps should be accessible by heating the surface above 150 °C.

Mapping the electronic structure of the diindenopyrene molecule

For a detailed investigation of the electronic structure, we recorded dI/dV maps at bias voltages corresponding to the resonances attributed to HOMO-1, HOMO, LUMO and LUMO+1 (Figure 5(a)). The two five-membered rings are expected to reduce the aromaticity of the DIP molecule.[21] Therefore, in the dI/dV maps, regions of higher differential conductance are located close to the DIP benzene moieties, while regions of lower differential conductance are located on the pentagonal rings. To further investigate the electronic structure of the DIP molecule, we have calculated constant-current dI/dV maps for a DIP molecule physisorbed on Au(111) by ESQC[36] at the corresponding tunneling electronic resonance energies, as presented in Figure 5(b). As one can see, the experimental differential conductance maps recorded at -1.3 V and +1.5 V are well reproduced by the ESQC mono-electronic approximation[36] indicating that the main molecular

orbital contribution to those resonances are coming from the HOMO and the LUMO molecular orbitals, respectively. Notice a little discrepancy between the experimental and calculated LUMO maps, certainly originated from a slightly different adsorption conformation of the DIP molecule used in the calculations. The separation of one lobe (experimental) to two lobes (calculated) on both sides of DIP in the LUMO maps was already observed on a Cu-phthalocyanine molecule. This difference comes probably from a slight deformation of the molecular skeleton at the hexagonal carbon ring.[37]

To theoretically simulate the -1.8 V and +2.45 V dI/dV maps, it was necessary to superpose several ESQC calculated DIP molecular orbital maps. This is an indication that those two resonances cannot be described solely by a single molecular orbital contribution of the corresponding many-body Slater determinants normally describing those resonances.[38] In particular, the -1.8 V dI/dV map can be fairly well reproduced by a weighted superposition of the calculated HOMO-2, HOMO-1 and HOMO dI/dV maps with a negative contribution from the HOMO, while the +2.45 V dI/dV map is a weighted superposition of the calculated LUMO+2 and LUMO+1 dI/dV maps (see Figure S4).

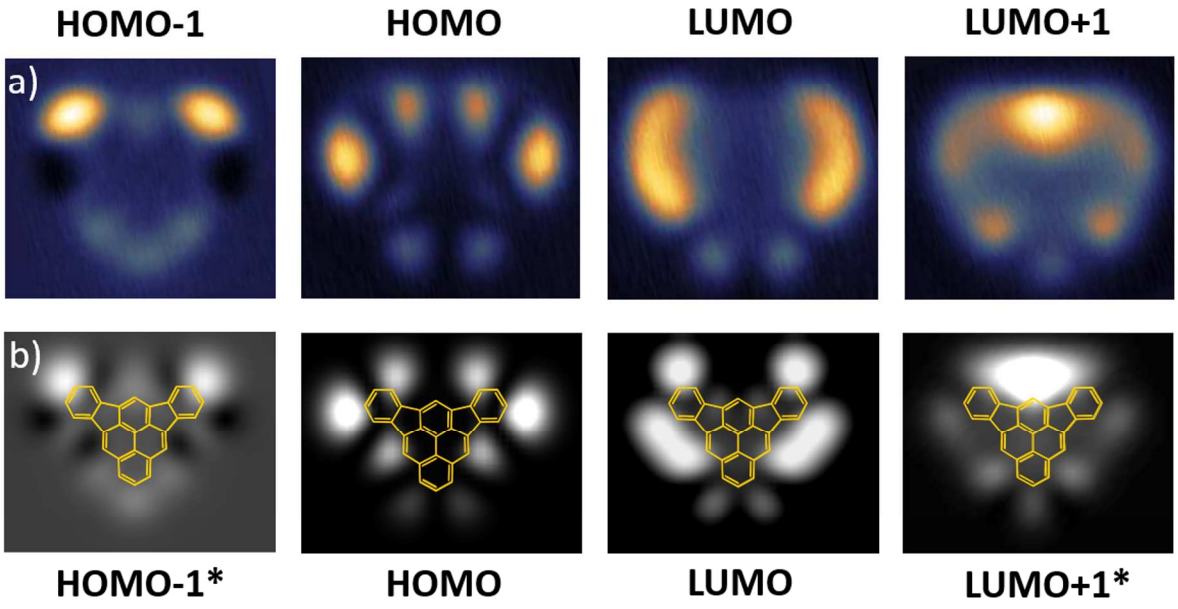

Figure 5. Mapping of the molecular orbital contribution of the DIP tunneling electronic resonances. (a) Experimental constant–current differential conductance maps recorded at the identified resonant bias values (HOMO-1: V = -1.8 V; HOMO: V = -1.3 V; LUMO: V = +1.5 V; LUMO+1: V = +2.45 V). Image sizes are 3.00 nm x 2.75 nm. Current for all images was 100 pA. (b) Calculated differential conductance maps at the corresponding energy resonances using mono-electronic elastic scattering quantum chemistry (ESQC). The HOMO-1* and LUMO+1* resonance maps were obtained by mixing multiple mono-electronic states to match the experimental observations (see Figure S4).

CONCLUSION

In summary, we report the on-surface synthesis of previously unknown diindeno[1,2,3-cd:1′,2′,3′-mn]pyrene molecule on Au(111). This intramolecular reaction makes use of the activation of the inner carbon scaffold by surface-assisted dehalogenation. Indene units, fused to the pyrene core, are formed *via* a regioselective cyclization pathway followed by methyl group migration and elimination. DFT modeling supports our experimental observations while the reaction mechanism is identified by NEB calculations. Moreover, the structure of the DIP molecules can be resolved by high-resolution STM images with a functionalized tip and the electronic structure investigated by scanning tunneling spectroscopy. Frontier orbital resonances

as well as HOMO-1 and LUMO+1, which resemble mixtures of several molecular resonances, are accessible with this technique and the calculated differential conductance maps show a striking agreement. Using such on-surface chemical approach in combination with proper design of molecular precursors should prove useful to access further non-alternant polyaromatic hydrocarbons.

METHODS

Experimental Details. Details on the synthesis of $Br_2Me_4Ph_2Py$ can be found in the Supporting Information. STM experiments were performed using a custom-built instrument operating at a low temperature of T ≈ 5 K and ultra-high vacuum (p ≈ 1 × 10^{-10} mbar) conditions. STM measurements were acquired in constant-current mode with the bias voltage applied to the sample. The high-resolution STM measurements were acquired in constant-height mode, and the tip apex was terminated with a CO molecule, which was picked up from the surface.[39] Differential conductance measurements were fulfilled with a metallic tip using lock-in detection with a modulation frequency of 833 Hz and a modulation amplitude of 20 mV. An Au(111) single crystal was used as substrate and prepared by repeated cycles of sputtering (Ar^+) and annealing (730 K). After this cleaning procedure, $Br_2Me_4Ph_2Py$ was evaporated from a Knudsen cell at a deposition temperature of 420 K. Temperature-induced experiments were carried out by annealing the sample at the respective temperature for 5 min after transferring it out of the STM

without breaking the ultra-high vacuum. Subsequently, the sample was cooled and transferred back again inside the STM.

Computational Details. Density functional theory (DFT) in a mixed Gaussian and plane wave scheme, as implemented in the Quickstep code of the CP2K package[40-42] was used to study the adsorption of individual molecules and understand the mechanism of the chemical reaction. We applied Perdew-Burke-Ernzerhof exchange-correlation functionals,[43] Goedecker-Teter-Hutter pseudo potentials[44] and a valence double-ζ basis set, together with the DFT-D3 method of Grimme[45] for van der Waals correction. The Au(111) substrate was modelled as a slab of three atomic gold layers with periodic boundary conditions, representing an infinite Au(111) surface. Full geometry optimizations were carried out for initial, intermediate and final reaction steps, with the lowest gold layer fixed. The reaction path was obtained by climbing image nudged-elastic band (CI-NEB) calculations,[46] which account for correct transition states. The reported barrier heights correspond to the system at 0 K, whereas finite temperature can lower the barriers due to dynamic effects. To confirm the final reaction product, the mono-electronic elastic scattering quantum chemistry (ESQC)[36] approach has been adopted to calculate constant-current dI/dV spectra and maps.

ASSOCIATED CONTENT

Supporting Information. Details on the synthesis of the precursor, additional STM data, as well as details on calculated differential conductance maps. This material is available free of charge on the ACS Publications website at http://pubs.acs.org.

The authors declare no competing financial interests.

AUTHOR INFORMATION

Corresponding Authors

E-mail: francesca.moresco@tu-dresden.de

ACKNOWLEDGEMENT

This work was funded by the ICT-FET European Union Integrated Project ATMOL and PAMS. Support by the German Excellence Initiative *via* the Cluster of Excellence EXC1056 ‘‘Center for Advancing Electronics Dresden’’ (cfaed), the International Helmholtz Research School ‘‘Nanonet’’, and the German Research Foundation (*via* SFB 951) is gratefully acknowledged. We further thank the Center for Information Services and High Performance Computing (ZIH) at TU Dresden for computational resources. T.L. gratefully acknowledges the International Excellence Graduate School on Emerging Materials and Processes Korea (iEGSEMP Korea) in the context of TU Dresden’s Institutional Strategy The Synergetic University.

REFERENCES

1. Lindner, R.; Kühnle, A., On-Surface Reactions. *ChemPhysChem* **2015,** *16*, 1582-1592.
2. Shen, Q.; Gao, H.-Y.; Fuchs, H., Frontiers of On-Surface Synthesis: From Principles to Applications. *Nano Today* **2017,** *13*, 77-96.
3. Mendez, J.; Lopez, M. F.; Martin-Gago, J. A., On-Surface Synthesis of Cyclic Organic Molecules. *Chem. Soc. Rev.* **2011,** *40*, 4578-4590.
4. Gourdon, A., On-Surface Covalent Coupling in Ultrahigh Vacuum. *Angew. Chem. Int. Ed.* **2008,** *47*, 6950-6953.
5. Hla, S.-W.; Bartels, L.; Meyer, G.; Rieder, K.-H., Inducing All Steps of a Chemical Reaction with the Scanning Tunneling Microscope Tip: Towards Single Molecule Engineering. *Phys. Rev.Lett.* **2000,** *85*, 2777-2780.

6. Grill, L.; Dyer, M.; Lafferentz, L.; Persson, M.; Peters, M. V.; Hecht, S., Nano-Architectures by Covalent Assembly of Molecular Building Blocks. *Nat. Nanotechnol.* **2007,** *2*, 687-691.
7. Lackinger, M., Surface-Assisted Ullmann Coupling. *Chem. Commun.* **2017,** *53*, 7872-7885.
8. Nacci, C.; Ample, F.; Bleger, D.; Hecht, S.; Joachim, C.; Grill, L., Conductance of a Single Flexible Molecular Wire Composed of Alternating Donor and Acceptor Units. *Nat. Commun.* **2015,** *6*, 7397.
9. Lafferentz, L.; Ample, F.; Yu, H.; Hecht, S.; Joachim, C.; Grill, L., Conductance of a Single Conjugated Polymer as a Continuous Function of Its Length. *Science* **2009,** *323*, 1193-1197.
10. Cai, J.; Ruffieux, P.; Jaafar, R.; Bieri, M.; Braun, T.; Blankenburg, S.; Muoth, M.; Seitsonen, A. P.; Saleh, M.; Feng, X.; Mullen, K.; Fasel, R., Atomically Precise Bottom-Up Fabrication of Graphene Nanoribbons. *Nature* **2010,** *466*, 470-473.
11. Ruffieux, P.; Wang, S.; Yang, B.; Sánchez-Sánchez, C.; Liu, J.; Dienel, T.; Talirz, L.; Shinde, P.; Pignedoli, C. A.; Passerone, D.; Dumslaff, T.; Feng, X.; Müllen, K.; Fasel, R., On-Surface Synthesis of Graphene Nanoribbons with Zigzag Edge Topology. *Nature* **2016,** *531*, 489-492.
12. Schuler, B.; Fatayer, S.; Mohn, F.; Moll, N.; Pavliček, N.; Meyer, G.; Peña, D.; Gross, L., Reversible Bergman Cyclization by Atomic Manipulation. *Nat. Chem.* **2016,** *8*, 220-224.
13. Pavliček, N.; Schuler, B.; Collazos, S.; Moll, N.; Pérez, D.; Guitián, E.; Meyer, G.; Peña, D.; Gross, L., On-Surface Generation and Imaging of Arynes by Atomic Force Microscopy. *Nat. Chem.* **2015,** *7*, 623-628.
14. Pavliček, N.; Gross, L., Generation, Manipulation and Characterization of Molecules by Atomic Force Microscopy. *Nat. Rev. Chem.* **2017,** *1*, 0005.
15. Kawai, S.; Takahashi, K.; Ito, S.; Pawlak, R.; Meier, T.; Spijker, P.; Canova, F. F.; Tracey, J.; Nozaki, K.; Foster, A. S.; Meyer, E., Competing Annulene and Radialene Structures in a Single Anti-Aromatic Molecule Studied by High-Resolution Atomic Force Microscopy. *ACS Nano* **2017,** *11*, 8122-8130.
16. Rogers, C.; Chen, C.; Pedramrazi, Z.; Omrani, A. A.; Tsai, H.-Z.; Jung, H. S.; Lin, S.; Crommie, M. F.; Fischer, F. R., Closing the Nanographene Gap: Surface-Assisted Synthesis of Peripentacene from 6,6′-Bipentacene Precursors. *Angew. Chem. Int. Ed.* **2015,** *54*, 15143-15146.
17. Pavliček, N.; Mistry, A.; Majzik, Z.; Moll, N.; Meyer, G.; Fox, D. J.; Gross, L., Synthesis and Characterization of Triangulene. *Nat. Nanotechnol.* **2017,** *12*, 308-311.
18. Krüger, J.; Eisenhut, F.; Alonso, J. M.; Lehmann, T.; Guitian, E.; Perez, D.; Skidin, D.; Gamaleja, F.; Ryndyk, D. A.; Joachim, C.; Pena, D.; Moresco, F.; Cuniberti, G., Imaging the Electronic Structure of On-Surface Generated Hexacene. *Chem. Commun.* **2017,** *53*, 1583-1586.
19. Liu, M.; Liu, M.; She, L.; Zha, Z.; Pan, J.; Li, S.; Li, T.; He, Y.; Cai, Z.; Wang, J.; Zheng, Y.; Qiu, X.; Zhong, D., Graphene-Like Nanoribbons Periodically Embedded with Four- and Eight-Membered Rings. *Nat. Commun.* **2017,** *8*, 14924.
20. Krüger, J.; García, F.; Eisenhut, F.; Skidin, D.; Alonso, J. M.; Guitián, E.; Pérez, D.; Cuniberti, G.; Moresco, F.; Peña, D., Decacene: On-Surface Generation. *Angew. Chem. Int. Ed.* **2017,** *56*, 11945-11948.
21. Havenith, R. W. A.; Jiao, H.; Jenneskens, L. W.; van Lenthe, J. H.; Sarobe, M.; Schleyer, P. v. R.; Kataoka, M.; Necula, A.; Scott, L. T., Stability and Aromaticity of the Cyclopenta-Fused Pyrene Congeners. *J. Am. Chem. Soc.* **2002,** *124*, 2363-2370.

22. Liu, J.; Dienel, T.; Liu, J.; Groening, O.; Cai, J.; Feng, X.; Müllen, K.; Ruffieux, P.; Fasel, R., Building Pentagons into Graphenic Structures by On-Surface Polymerization and Aromatic Cyclodehydrogenation of Phenyl-Substituted Polycyclic Aromatic Hydrocarbons. *J. Phys. Chem. C* **2016,** *120*, 17588-17593.
23. Tebi, S.; Paszkiewicz, M.; Aldahhak, H.; Allegretti, F.; Gonglach, S.; Haas, M.; Waser, M.; Deimel, P. S.; Aguilar, P. C.; Zhang, Y.-Q.; Papageorgiou, A. C.; Duncan, D. A.; Barth, J. V.; Schmidt, W. G.; Koch, R.; Gerstmann, U.; Rauls, E.; Klappenberger, F.; Schöfberger, W.; Müllegger, S., On-Surface Site-Selective Cyclization of Corrole Radicals. *ACS Nano* **2017,** *11*, 3383-3391.
24. de Oteyza, D. G.; Gorman, P.; Chen, Y.-C.; Wickenburg, S.; Riss, A.; Mowbray, D. J.; Etkin, G.; Pedramrazi, Z.; Tsai, H.-Z.; Rubio, A.; Crommie, M. F.; Fischer, F. R., Direct Imaging of Covalent Bond Structure in Single-Molecule Chemical Reactions. *Science* **2013,** *340*, 1434.
25. de Oteyza, D. G.; Pérez Paz, A.; Chen, Y.-C.; Pedramrazi, Z.; Riss, A.; Wickenburg, S.; Tsai, H.-Z.; Fischer, F. R.; Crommie, M. F.; Rubio, A., Noncovalent Dimerization after Enediyne Cyclization on Au(111). *J. Am. Chem. Soc.* **2016,** *138*, 10963-10967.
26. Kawai, S.; Haapasilta, V.; Lindner, B. D.; Tahara, K.; Spijker, P.; Buitendijk, J. A.; Pawlak, R.; Meier, T.; Tobe, Y.; Foster, A. S.; Meyer, E., Thermal Control of Sequential On-Surface Transformation of a Hydrocarbon Molecule on a Copper Surface. *Nat. Commun.* **2016,** *7*, 12711.
27. Wegner, H. A.; Reisch, H.; Rauch, K.; Demeter, A.; Zachariasse, K. A.; de Meijere, A.; Scott, L. T., Oligoindenopyrenes: A New Class of Polycyclic Aromatics. *J. Org. Chem.* **2006,** *71*, 9080-9087.
28. de Oteyza, D. G.; García-Lekue, A.; Vilas-Varela, M.; Merino-Díez, N.; Carbonell-Sanromà, E.; Corso, M.; Vasseur, G.; Rogero, C.; Guitián, E.; Pascual, J. I.; Ortega, J. E.; Wakayama, Y.; Peña, D., Substrate-Independent Growth of Atomically Precise Chiral Graphene Nanoribbons. *ACS Nano* **2016,** *10*, 9000-9008.
29. Batra, A.; Cvetko, D.; Kladnik, G.; Adak, O.; Cardoso, C.; Ferretti, A.; Prezzi, D.; Molinari, E.; Morgante, A.; Venkataraman, L., Probing the Mechanism for Graphene Nanoribbon Formation on Gold Surfaces through X-Ray Spectroscopy. *Chem. Sci.* **2014,** *5*, 4419-4423.
30. Bieri, M.; Nguyen, M.-T.; Gröning, O.; Cai, J.; Treier, M.; Aït-Mansour, K.; Ruffieux, P.; Pignedoli, C. A.; Passerone, D.; Kastler, M.; Müllen, K.; Fasel, R., Two-Dimensional Polymer Formation on Surfaces: Insight into the Roles of Precursor Mobility and Reactivity. *J. Am. Chem. Soc.* **2010,** *132*, 16669-16676.
31. Nacci, C.; Hecht, S.; Grill, L., The Emergence of Covalent On-Surface Polymerization. In *On-Surface Synthesis: Proceedings of the International Workshop On-Surface Synthesis, École des Houches, Les Houches 25-30 May 2014*, Gourdon, A., Ed. Springer International Publishing: Cham, 2016; pp 1-21.
32. Dong, L.; Wang, S.; Wang, W.; Chen, C.; Lin, T.; Adisoejoso, J.; Lin, N., Transition Metals Trigger On-Surface Ullmann Coupling Reaction: Intermediate, Catalyst and Template. In *On-Surface Synthesis: Proceedings of the International Workshop On-Surface Synthesis, École des Houches, Les Houches 25-30 May 2014*, Gourdon, A., Ed. Springer International Publishing: Cham, 2016; pp 23-42.
33. Gross, L.; Moll, N.; Mohn, F.; Curioni, A.; Meyer, G.; Hanke, F.; Persson, M., High-Resolution Molecular Orbital Imaging Using a p-Wave STM Tip. *Phys. Rev. Lett.* **2011,** *107*, 086101.

34. Björk, J.; Hanke, F.; Stafström, S., Mechanisms of Halogen-Based Covalent Self-Assembly on Metal Surfaces. *J. Am. Chem. Soc.* **2013,** *135*, 5768-5775.
35. Scott, L. T., Chemistry at the Interior Atoms of Polycyclic Aromatic Hydrocarbons. *Chem. Soc. Rev.* **2015,** *44*, 6464-6471.
36. Sautet, P.; Joachim, C., Calculation of the Benzene on Rhodium STM Images. *Chem. Phys. Lett.* **1991,** *185*, 23-30.
37. Soe, W. H.; Manzano, C.; Wong, H. S.; Joachim, C., Mapping the First Electronic Resonances of a Cu Phthalocyanine STM Tunnel Junction. *J. Phys.: Condens. Matter* **2012,** *24*, 354011.
38. Portais, M.; Joachim, C., Hole–Electron Quantum Tunnelling Interferences through a Molecular Junction. *Chem. Phys. Lett.* **2014,** *592*, 272-276.
39. Bartels, L.; Meyer, G.; Rieder, K. H., Controlled Vertical Manipulation of Single CO Molecules with the Scanning Tunneling Microscope: A Route to Chemical Contrast. *Appl. Phys. Lett.* **1997,** *71*, 213-215.
40. Hohenberg, P.; Kohn, W., Inhomogeneous Electron Gas. *Phys. Rev.* **1964,** *136*, B864-B871.
41. Kohn, W.; Sham, L. J., Self-Consistent Equations Including Exchange and Correlation Effects. *Phys. Rev.* **1965,** *140*, A1133-A1138.
42. VandeVondele, J.; Krack, M.; Mohamed, F.; Parrinello, M.; Chassaing, T.; Hutter, J., Quickstep: Fast and Accurate Density Functional Calculations Using a Mixed Gaussian and Plane Waves Approach. *Comput. Phys. Commun.* **2005,** *167*, 103-128.
43. Perdew, J. P.; Burke, K.; Ernzerhof, M., Generalized Gradient Approximation Made Simple. *Phys. Rev. Lett.* **1996,** *77*, 3865-3868.
44. Goedecker, S.; Teter, M.; Hutter, J., Separable Dual-Space Gaussian Pseudopotentials. *Phys. Rev. B* **1996,** *54*, 1703-1710.
45. Grimme, S.; Antony, J.; Ehrlich, S.; Krieg, H., A Consistent and Accurate *Ab Initio* Parametrization of Density Functional Dispersion Correction (DFT-D) for the 94 Elements H-Pu. *J. Chem. Phys.* **2010,** *132*, 154104.
46. Henkelman, G.; Uberuaga, B. P.; Jónsson, H., A Climbing Image Nudged Elastic Band Method for Finding Saddle Points and Minimum Energy Paths. *J. Chem. Phys.* **2000,** *113*, 9901-9904.

For Table of Contents only